Diagn Interv Radiol 2026; DOI: 10.4274/dir.2026.264132

NEURORADIOLOGY

INVITED REVIEW

©Copyright 2026 Author(s) - Available online at dirjournal.org.
Content of this journal is licensed under a Creative Commons Attribution-NonCommercial 4.0 International License.

Beyond the flow: the evolving role of magnetic resonance imaging in arteriovenous shunt evaluation

Akihiko Sakata[1]
Koji Fujimoto[2]
Mami Iima[3]
Tsukasa Saida[4]
Kentaro Nishioka[5]
Rintaro Ito[6]
Maya Honda[7]
Masahiro Yanagawa[8]
Ryo Kurokawa[9]
Kenji Hirata[10]
Mariko Kawamura[11]
Seitaro Oda[12]
Satoru Ide[13]
Shunsuke Sugawara[14]
Koji Takumi[15]
Daiju Ueda[16]
Keitaro Sofue[17]
Shinji Naganawa[11]

[1]Kyoto University Graduate School of Medicine, Department of Diagnostic Imaging and Nuclear Medicine, Kyoto, Japan
[2]Hamamatsu University School of Medicine, Department of Advanced Healthcare Informatics, Shizuoka, Japan
[3]Nagoya University Graduate School of Medicine, Department of Fundamental Development for Advanced Low Invasive Diagnostic Imaging, Aichi, Japan
[4]University of Tsukuba, Department of Radiology, Ibaraki, Japan
[5]Hokkaido University Faculty of Medicine, Division of Radiation Oncology, Global Center for Biomedical Science and Engineering, Hokkaido, Japan
[6]Nagoya University Graduate School of Medicine, Department of Innovative BioMedical Visualization, Nagoya, Japan
[7]Kyoto University Hospital, Preemptive Medicine and Lifestyle-Related Disease Research Center, Kyoto, Japan
[8]The University of Osaka Graduate School of Medicine, Department of Radiology, Osaka, Japan
[9]The University of Tokyo Graduate School of Medicine, Department of Radiology, Tokyo, Japan
[10]Hokkaido University Faculty of Medicine, Department of Diagnostic Imaging, Hokkaido, Japan
[11]Nagoya University Graduate School of Medicine, Department of Radiology, Aichi, Japan
[12]Kumamoto University Faculty of Life Sciences, Department of Diagnostic Radiology, Kumamoto, Japan
[13]University of Occupational and Environmental Health, Department of Radiology, Fukuoka, Japan
[14]National Cancer Center Hospital, Department of Diagnostic Radiology, Tokyo, Japan
[15]Kagoshima University Graduate School of Medical and Dental Sciences, Department of Radiology, Kagoshima, Japan
[16]Osaka Metropolitan University Graduate School of Medicine, Department of Artificial Intelligence, Osaka, Japan
[17]Kobe University Graduate School of Medicine, Department of Radiology, Hyogo, Japan

ABSTRACT

Although digital subtraction angiography remains the gold standard for the diagnosis and treatment planning of intracranial arteriovenous shunts (AVS), including arteriovenous malformations and arteriovenous fistulas, non-invasive imaging is increasingly sought for comprehensive evaluation. Magnetic resonance imaging (MRI) plays a crucial role in AVS detection, identification of feeding arteries and draining veins, localization of shunt points, classification of subtypes, assessment of venous reflux and congestion, and evaluation of post-treatment residual or recurrent lesions. Clinical techniques such as time-of-flight MR angiography (MRA), contrast-enhanced time-resolved MRA, susceptibility-weighted imaging, and arterial spin labeling (ASL) are established for these assessments. Recent advances have expanded MRI capabilities: Ultrashort echo time MRA can overcome turbulent flow-related signal loss and susceptibility artifacts, improving visualization of complex nidus architecture; compressed sensing substantially accelerates three-dimensional and four-dimensional (4D)-MRA while maintaining diagnostic quality; ASL-based 4D-MRA provides high-temporal-resolution dynamic evaluation without contrast, with vessel-selective techniques enabling independent assessment of individual vascular territories; and high-resolution vessel wall imaging shows promise for risk stratification. Emerging artificial intelligence applications enable automated AVS segmentation and characterization, with potential to enhance image quality and reduce scan times. This review summarizes current MRI techniques, recent innovations, and future perspectives in the non-invasive assessment of intracranial AVS.

KEYWORDS

Arterial spin labeling, arteriovenous fistula, arteriovenous malformation, artificial intelligence, compressed sensing, MRA, susceptibility-weighted imaging, ultrashort echo time MRA, vessel wall imaging

Handling editor: Nurullah Dağ

Corresponding author: Akihiko Sakata

E-mail: asakata@kuhp.kyoto-u.ac.jp

Received 21 May 2026; revision requested 06 June 2026; accepted 04 July 2026.

Epub: 05.08.2026

DOI: 10.4274/dir.2026.264132

You may cite this article as: Sakata A, Fujimoto K, Iima M, et al. Beyond the flow: the evolving role of magnetic resonance imaging in arteriovenous shunt evaluation. *Diagn Interv Radiol*. 05 August 2026 DOI: 10.4274/dir.2026.264132 [Epub Ahead of Print].

Cerebral arteriovenous shunts (AVS), including brain arteriovenous malformations (AVMs) and dural arteriovenous fistulas (DAVFs), represent a heterogeneous group of vascular disorders characterized by direct arteriovenous connections without an intervening capillary bed.[1,2] These lesions exhibit highly variable angioarchitectures and clinical behaviors, ranging from incidental asymptomatic findings to aggressive presentations with intracranial hemorrhage, progressive neurological deficits, or venous hypertensive encephalopathy. Treatment strategies—such as microsurgical resection, endovascular embolization, stereotactic radiosurgery, or conservative observation—are critically dependent on accurate characterization of shunt angioarchitecture and its hemodynamic impact on the brain. Imaging is therefore indispensable for initial diagnosis and treatment planning. It also plays a critical role in post-treatment evaluation and long-term surveillance for disease recurrence or progression.

Digital subtraction angiography (DSA) has long been regarded as the gold standard for the evaluation of cerebral AVS. Its unparalleled spatial and temporal resolution enables accurate visualization of the angioarchitectural features central to established classification systems, including nidus size, eloquence of the adjacent brain, and venous drainage patterns in the Spetzler–Martin grading of AVMs[3] and the presence of cortical venous reflux (CVR), also termed retrograde leptomeningeal venous drainage (RLVD), in the Borden and Cognard classifications of DAVFs (Table 1).[4,5] CVR/RLVD arises when shunt-induced venous hypertension reverses normal venous drainage into cortical and leptomeningeal veins, and its presence identifies a lesion at higher risk of hemorrhage and venous congestion. DSA also allows real-time hemodynamic assessment and serves as both a diagnostic and therapeutic platform, forming the basis of contemporary endovascular treatment. However, despite these advantages, DSA has inherent limitations. It is an invasive procedure associated with complications such as ischemic stroke, requires iodinated contrast media, and involves radiation exposure. These factors make frequent or longitudinal follow-up with DSA impractical, particularly in patients requiring repeated follow-up or those with stable or conservatively managed lesions. Furthermore, following the ARUBA trial,[6] which demonstrated that conservative management may be preferable to intervention for unruptured AVMs, there has been growing interest in managing selected patients conservatively, further highlighting the clinical need for reliable non-invasive imaging for long-term surveillance.

In this context, magnetic resonance angiography (MRA) has assumed an increasingly important complementary role in AVS evaluation. As a non-invasive technique that requires no ionizing radiation and can be safely repeated, MRA is particularly suitable for longitudinal monitoring. It enables visualization of feeding arteries, draining veins, and shunt architecture, facilitating risk stratification and post-treatment evaluation.[7] Beyond vascular assessment, MR imaging (MRI) also provides a comprehensive evaluation of the brain parenchyma, not only providing complementary information regarding the relationship of the nidus to eloquent brain regions but also allowing the detection of venous congestion, edema, ischemic changes, or prior hemorrhage. These findings directly reflect the biological impact of AVS and often play a critical role in clinical risk stratification, especially in DAVFs, where venous hypertension determines neurological prognosis.[8]

Nevertheless, MRA techniques have well-recognized limitations compared with DSA. Spatial and temporal resolution remain insufficient for detailed characterization of complex shunt angioarchitecture, and small or slow-flow shunts may be overlooked.[9] Hemodynamic assessment has traditionally relied on contrast-enhanced (CE) techniques, and evaluation of venous congestion has required additional sequences beyond conventional MRA. In recent years, several

Main points

- Recent advances in magnetic resonance (MR) imaging techniques have improved the visualization and characterization of arteriovenous shunts.
- Advances in non-contrast MR angiography (MRA) techniques enable detailed structural visualization of complex vascular anatomy within relatively short acquisition times.
- Innovations in contrast-enhanced time-resolved MRA have achieved both noise reduction and improved temporal resolution for superior dynamic assessment.
- High-resolution vessel wall imaging enables *in vivo* assessment of vascular wall pathology, providing insights into rupture risk and disease activity beyond conventional luminal anatomy.
- Artificial intelligence applications, including deep learning-based reconstruction and automated segmentation, are emerging as promising tools for improving diagnostic accuracy and workflow efficiency in the evaluation of arteriovenous shunts.

Table 1. Common angiographic grading and classification systems for brain AVMs and dural AVFs

Classification system	Grade/type	Criteria
Spetzler–Martin grading of brain AVMs	Grades I–V (sum of points)	Nidus size: < 3 cm = 1; 3–6 cm = 2; > 6 cm = 3. Eloquence of the adjacent brain: non-eloquent = 0; eloquent = 1. Venous drainage: superficial only = 0; any deep component = 1. Grade = sum of the three component scores.
Borden classification of DAVFs	Type I	Drainage into a dural venous sinus or meningeal vein with antegrade flow; no cortical venous reflux.
	Type II	Drainage into a dural venous sinus with cortical venous reflux.
	Type III	Direct drainage into cortical/leptomeningeal veins without dural sinus drainage.
Cognard classification of DAVFs	Type I	Dural sinus drainage with antegrade flow; no cortical venous reflux.
	Type IIa	Dural sinus drainage with retrograde sinus flow; no cortical venous reflux.
	Type IIb	Dural sinus drainage with antegrade flow and cortical venous reflux.
	Type IIa + b	Dural sinus drainage with retrograde sinus flow and cortical venous reflux.
	Type III	Direct cortical venous drainage without venous ectasia.
	Type IV	Direct cortical venous drainage with venous ectasia.
	Type V	Spinal perimedullary venous drainage.

The Spetzler–Martin grade is primarily a surgical risk grading system for brain AVMs and does not necessarily predict the risks associated with embolization or radiosurgery. In DAVFs, cortical venous drainage/reflux is the key feature associated with aggressive clinical behavior, including hemorrhage and non-hemorrhagic neurological deficits. When used, the optional Borden suffixes a and b denote single-hole (simple) and multiple-hole (complex) fistulous architecture, respectively. AVM, arteriovenous malformation; DAVF, dural arteriovenous fistula.

novel complementary techniques, including non-contrast approaches and advanced acquisition strategies, have been developed to address these shortcomings, progressively expanding the diagnostic scope of non-invasive AVS evaluation.[10-12] Moreover, the advent of vessel wall imaging (VWI) has provided unique insights into VW pathology and disease activity that were previously inaccessible with conventional angiographic assessment.[13]

The purpose of this review is to summarize recent advances in MRI-based imaging of cerebral AVS, with a focus on how emerging techniques may complement conventional MRA. Whereas previous reviews have largely centered on established MRA techniques, the present review emphasizes the most recent innovations—ultrashort echo time (UTE)-MRA, compressed sensing (CS) acceleration, vessel-selective arterial spin labeling (ASL)-based four-dimensional (4D)-MRA, VWI, and artificial intelligence (AI)—and frames them within a practical perspective oriented toward non-invasive, longitudinal management of AVS. Table 2 provides a comprehensive summary of these techniques. By clarifying both the current capabilities and the remaining challenges of MRI in this field, we aim to highlight its evolving role in the comprehensive management of AVS.

Clinical magnetic resonance techniques for arteriovenous shunt

Time-of-flight magnetic resonance angiography

Principle

Time-of-flight MRA (TOF-MRA) is a flow-dependent technique that exploits differences in magnetization between stationary tissue and flowing blood without requiring exogenous contrast agents.[14] Radiofrequency pulses repeatedly applied within the imaging volume saturate stationary tissue, whereas fresh arterial blood flowing into the imaging volume retains high longitudinal magnetization and appears hyperintense against the suppressed background.

Diagnostic performance

TOF-MRA has been widely used for the evaluation of intracranial AVS (Figures 1 and 2, Supplementary Videos 1–4), with diagnostic performance that has evolved substantially with advances in field strength. In clinical practice, maximum intensity projection (MIP) images are frequently used for efficient image interpretation, providing an intuitive overview of the vascular architecture. Early reports using 1.5T systems demonstrated that nidus topography was reasonably well appreciated on TOF-MRA; however, hyperdynamic feeding arteries were incompletely depicted, and venous structures were poorly visualized because of saturation effects.[9] The transition to 3T has substantially improved diagnostic performance: Signal-to-noise ratios (SNRs) are approximately twice those of 1.5T, and prolonged T1 relaxation times enhance background suppression and vessel-to-tissue contrast. Studies have demonstrated that 3T TOF-MRA detects 21% more feeding arteries and 33% more deep draining veins than 1.5T,[15] facilitating the detection of arteriovenous fistulas, particularly at dural locations.[16]

Table 2. Overview of clinical and emerging MRI techniques for AVS

Technique	Contrast agent	Temporal resolution	Key clinical strength	Post-treatment utility	Key limitation
Clinical MR techniques					
TOF-MRA	No	None (static)	Widely available baseline screening	Low sensitivity for residual nidus	Slow flow/venous signal loss
CE TR-MRA	Yes	Intermediate (2–6 s)	Hemodynamic assessment	Limited by susceptibility artifacts	One-shot acquisition/lower temporal resolution
ASL (perfusion)	No	None (static)	High-sensitivity shunt without contrast	Effective for residual shunt detection	Inherently low SNR
SWI	No	None (static)	AVS detection (hyperintense veins), venous congestion/CVR, and microhemorrhages	Tracking gradual shunt obliteration (signal reduction) and resolution of congestion	Artifacts at air–bone interfaces (skull base), blooming (coils/hemorrhage), and may miss slow-flow shunts
Recent technical innovations					
UTE-MRA	No	None (static)	Robust to turbulence and metallic artifact	Minimal artifact near coils	Lacks temporal resolution
CS-TOF-MRA	No	None (static)	Fast whole-brain coverage with high resolution	Efficient surveillance of extensive lesions	Sparse sampling artifacts
IT-TWIST	Yes	Very high (approximately 1.1 s)	Hemodynamic assessment with minimal gadolinium	Ideal for safe repeated surveillance	Still requires IV access/ghosting artifact
GRASP	Yes	High (1–2 s)	Continuous free-breathing acquisition	Robust against motion artifacts	Requires intensive reconstruction
ASL 4D-MRA	No	Very high (0.25–1 s)	Non-contrast dynamic, vessel-selective mapping	Excellent for safe, repeated surveillance	Long scan times; delayed signal decay
VW-MRI	Yes	None (static)	Wall pathology/rupture risk stratification	Detecting residual active inflammation	Long scan; interpretation variability

AVS, arteriovenous shunt; TOF-MRA, time-of-flight magnetic resonance angiography; CE TR-MRA, contrast-enhanced time-resolved magnetic resonance angiography; ASL, arterial spin labeling; SWI, susceptibility-weighted imaging; UTE-MRA, ultrashort echo time magnetic resonance angiography; CS, compressed sensing; IT-TWIST, Iterative reconstruction-based Time-resolved angiography with Interleaved Stochastic Trajectories; GRASP, golden-angle radial sparse parallel imaging; VW-MRI, vessel wall magnetic resonance imaging; CVR, cortical venous reflux, SNR, signal-to-noise ratio.

Limitations

TOF-MRA has well-recognized inherent weaknesses. Signal loss in regions of turbulent or slow flow remains problematic, rendering draining veins highly prone to incomplete depiction. The lack of temporal resolution precludes hemodynamic analysis and results in poor sensitivity for detecting treatment-related obliteration.[17] Furthermore, physiologic jugular venous reflux can mimic cavernous dural AVFs on TOF-MRA (Figure 3), as retrograde flow in the inferior petrosal and cavernous sinuses creates imaging findings that overlap with those of true AVS.[18]

Practical tips for source image interpretation

Although MIP images provide a convenient overview of vascular anatomy and are commonly used for initial evaluation, careful attention to source images is essential to overcome the limitations and pitfalls of TOF-MRA. Asymmetric enlargement of external carotid artery branches—including the middle meningeal, ascending pharyngeal, accessory meningeal, and occipital arteries—on source images provides important clues for distinguishing true DAVFs from physiologic jugular venous reflux (Figure 4), a distinction that MIP algorithms may obscure.[19] For superior sagittal sinus fistulas specifically, recognizing abnormal prominence of the middle meningeal artery is a key diagnostic clue, as reflected in signs such as the middle meningeal artery sign (Figure 5).[20] Source image review is therefore essential in the evaluation of any suspected AVS with TOF-MRA.

Contrast-enhanced time-resolved four-dimensional magnetic resonance angiography

Principle

CE time-resolved MRA (CE TR-MRA) integrates temporal resolution with 3D spatial resolution to visualize the dynamic passage of blood through the cerebrovascular system. Conventional CE TR-MRA establishes the baseline for dynamic MRI evaluation by using techniques such as keyhole imaging, parallel imaging, and k-space undersampling [e.g., TR Imaging of Contrast Kinetics (GE Healthcare), TR angiography with Interleaved Stochastic Trajectories (TWIST) (Siemens Healthineers), and 4D TR Angiography using Keyhole (Philips Healthcare)] to generate multiphasic volumetric datasets with temporal resolutions ranging from 2 to 6 seconds and submillimeter isotropic spatial resolution.[21] This allows separation of the arterial, capillary, and venous phases, enabling detection of early venous drainage and differentiation of arterial feeders from draining veins—assessments that are impossible with static sequences.[22] In this review, MR-DSA refers to a dynamic, projectional angiographic representation—analogous to conventional catheter DSA—obtained from TR-MRA data by subtracting an appropriate reference: a pre-contrast mask for CE acquisitions or the control image of each label–control pair for ASL-based acquisitions. Magnetic resonance DSA thus denotes a mode of representation rather than a specific acquisition and is not synonymous with 4D-MRA; the underlying technique [e.g., TWIST, Golden-angle RAdial Sparse Parallel (GRASP), or ASL-based modified Asymmetric Signal Targeting with Alternating Radiofrequency (mASTAR)] is indicated in the corresponding figure and video legends.

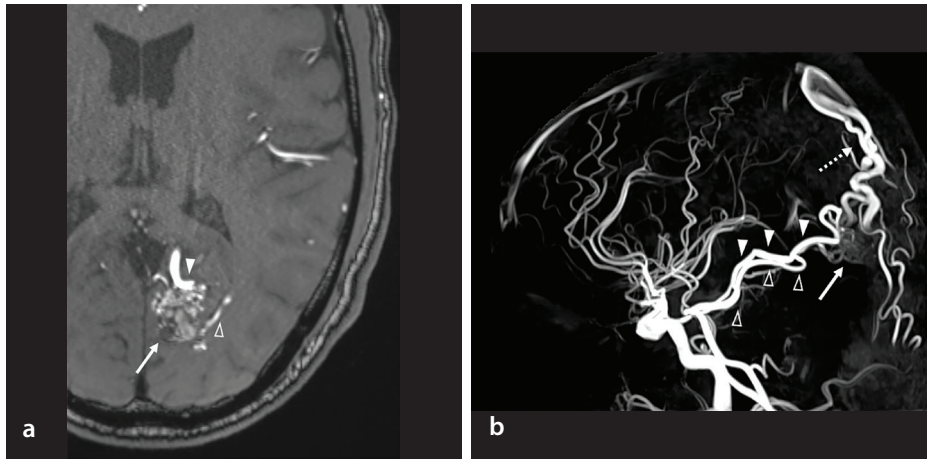

Figure 1. A 50-year-old man with a left cerebral AVM (Spetzler–Martin grade II) in the cuneus. On the TOF-MRA source image **(a)**, the feeding arteries (the parieto-occipital artery, arrowheads, and the calcarine artery, open arrowheads) and the nidus (19 mm in diameter, arrow) were visible in the cuneus. On the sagittal MIP reformation **(b)**, these same feeding arteries (arrowheads and open arrowheads) and the nidus (arrow) were demonstrated, together with the draining vein ascending along the parieto-occipital sulcus toward the superior sagittal sinus (dotted arrow); however, both the nidus and the draining vein were less well depicted than on DSA (Supplementary Video 1) and MR-DSA (Supplementary Video 2). AVM, arteriovenous malformation; TOF-MRA, time-of-flight magnetic resonance angiography; MIP, maximum intensity projection; MR-DSA, magnetic resonance-digital subtraction angiography.

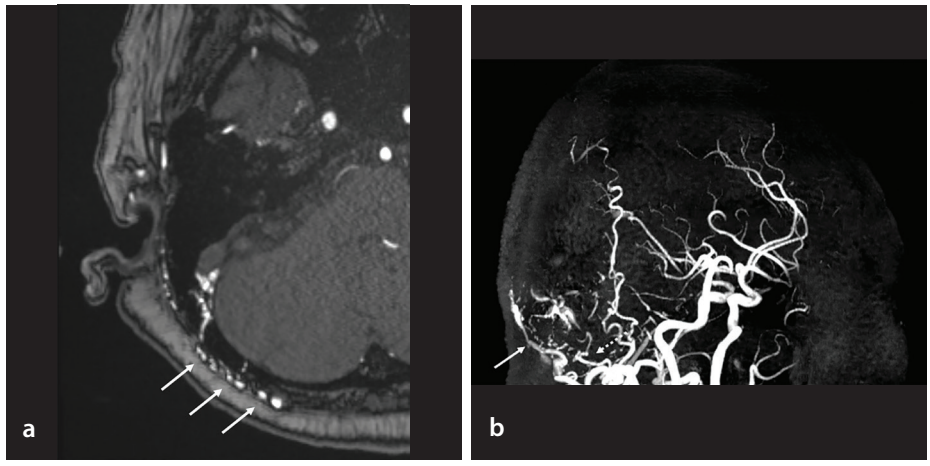

Figure 2. A 67-year-old woman with a right transverse-sigmoid sinus DAVF (Cognard classification type IIb). On the axial TOF-MRA image **(a)**, the transosseous feeders (white arrow) from the occipital artery and the shunting point at the right transverse-sigmoid junction were visible. On the sagittal MIP reformation **(b)**, the feeding arteries—the occipital artery (white arrow) and the posterior auricular artery (dotted arrow)—were clearly demonstrated; however, the draining veins were poorly visualized compared with DSA (Supplementary Video 3) and MR-DSA (Supplementary Video 4). DAVF, dural arteriovenous fistula; TOF-MRA, time-of-flight magnetic resonance angiography; MIP, maximum intensity projection; MR-DSA, magnetic resonance-digital subtraction angiography.

Diagnostic performance

CE TR-MRA has demonstrated high concordance with DSA across the spectrum of AVS (Supplementary Videos 1–4). For cerebral AVMs, detection rates of 89%–100% have been reported, with concordance rates of 93%–100% for Spetzler–Martin grading.[23] Angioarchitectural assessment shows good agreement with DSA for nidus size and venous drainage (κ: 0.75–0.77), although agreement is more modest for arterial feeders (κ: 0.44). For cranial DAVFs, fistula identification shows high correlation with DSA, whereas concordance for Cognard grading is somewhat lower, at 77%–93%, reflecting the inherent challenge of classifying complex drainage patterns non-invasively. Post-treatment surveillance demonstrates concordance of approximately 89% for residual nidus detection following surgery, embolization, or radiosurgery, with false-negative findings occurring predominantly in small, previously embolized lesions.[23]

Limitations

Despite these strengths, CE TR-MRA has important limitations that constrain its broader use. First, it requires intravenous gadolinium-based contrast agents, which have implications for patients with renal impairment and raise concerns regarding gadolinium deposition with repeated examinations. Second, CE TR-MRA is a single-opportunity acquisition: Once the contrast bolus has passed, the examination cannot be repeated without additional contrast administration. This one-shot nature demands precise scan timing and limits the ability to reacquire inadequate studies, a constraint that continuous k-space sampling approaches such as GRASP are designed to address.[24] Third, spatial and temporal resolution remain inferior to those of DSA, and susceptibility artifacts from liquid embolic agents or surgical clips can limit post-treatment evaluation. These limitations have motivated the development of alternative approaches, including CS–based techniques and non-contrast methods such as ASL-based MRA, as discussed in the following sections.

Arterial spin labeling

Principle

ASL is a non-invasive perfusion MRI technique that quantifies cerebral blood flow using arterial blood water as an endogenous contrast agent.[25,26] The basic principle involves magnetically labeling inflowing arterial blood protons using radiofrequency pulses (inversion) at a location proximal to the imaging volume (e.g., the neck). After a delay (post-labeling delay) to allow the labeled blood to reach the tissue of interest, labeled images are acquired. These are subtracted from control images (in which no labeling occurs), eliminating the static tissue signal and leaving a map proportional to cerebral perfusion.[25] The two primary labeling strategies are pulsed ASL (PASL) and pseudo-continuous ASL (PCASL), with PCASL generally recommended for clinical use because of its higher SNR.[27]

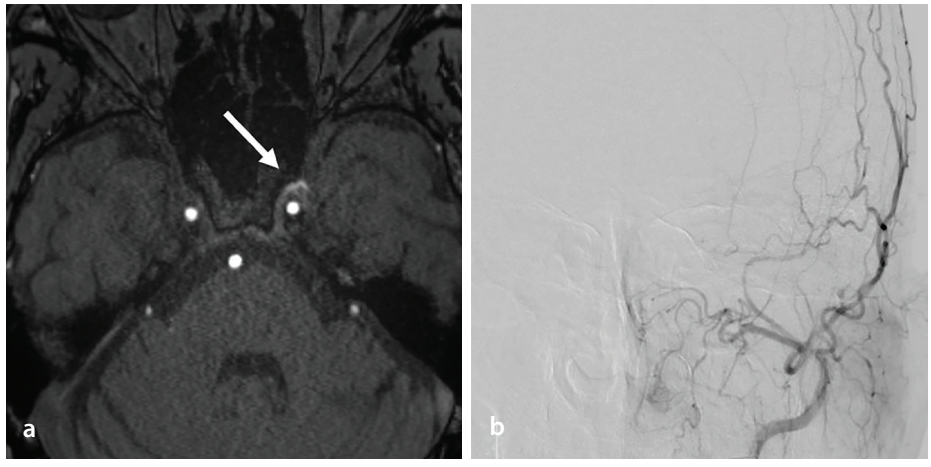

Figure 3. A 56-year-old man presenting with headache, in whom MRI raised suspicion of a left cavernous sinus DAVF. On the TOF-MRA source image **(a)**, abnormal signal was noted around the left cavernous sinus (arrow), without enlargement of the middle meningeal artery. On DSA performed for further workup (b, left external carotid artery injection), no definite arteriovenous shunting was identified, and the signal on TOF-MRA was attributed to physiologic venous flow within the cavernous sinus. MRI, magnetic resonance imaging; DAVF, dural arteriovenous fistula; TOF-MRA, time-of-flight magnetic resonance angiography; DSA, digital subtraction angiography.

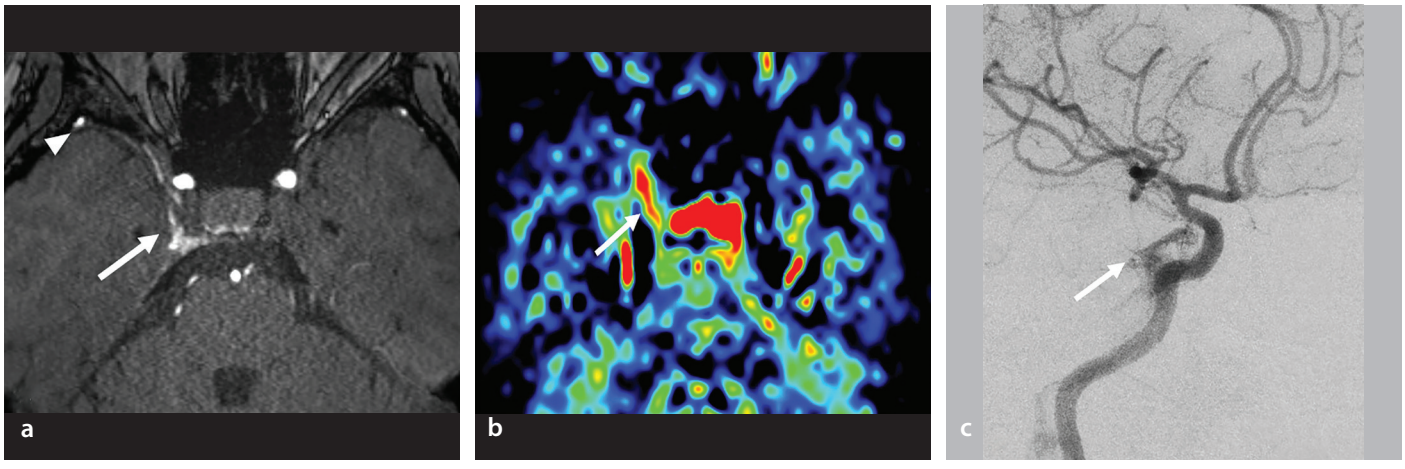

Figure 4. A 57-year-old woman presenting with progressive headache, retro-orbital pain, and oculomotor palsy, diagnosed with a right cavernous sinus DAVF (Cognard type I, Borden type **I**). On the TOF-MRA source image **(a)**, a flow signal was detected at the corresponding site (arrow), with enlargement of the right middle meningeal artery (arrowhead). On the ASL image **(b)**, markedly increased signal intensity at the shunting point was consistent with high flow through the DAVF (arrow). On 3D-DSA from the right ICA injection **(c)**, the shunt was identified lateral to the cavernous ICA (arrow). DAVF, dural arteriovenous fistula; TOF-MRA, time-of-flight magnetic resonance angiography; ASL, arterial spin labeling; 3D-DSA, three-dimensional digital subtraction angiography; ICA, internal carotid artery.

The greatest clinical advantage of ASL is its non-invasive nature. It requires no ionizing radiation or intravenous gadolinium contrast, making it safe for pediatric patients, women who are pregnant, and patients with renal failure or contrast allergies.

Diagnostic performance

In the context of AVS, ASL provides unique functional information by exploiting the rapid arteriovenous transit inherent to shunting lesions. Labeled blood bypassing the capillary bed transits rapidly into the venous system before substantial T1 decay occurs, resulting in a characteristic focal hyperintense signal within the nidus and draining veins on ASL perfusion maps [Figures 4(b) and 6(b)]. This feature makes ASL highly sensitive for AVS detection.[28,29] ASL is also valuable for post-treatment monitoring, particularly after stereotactic radiosurgery, where obliteration is gradual; it has demonstrated high sensitivity and specificity for residual shunt detection, potentially reducing the frequency of invasive DSA during follow-up.[10,30] Furthermore, ASL can assess the hemodynamic impact on the surrounding brain parenchyma, including hypoperfusion due to the steal phenomenon.[31,32] Beyond perfusion quantification, ASL can also serve as a non-contrast, TR angiographic technique, and its application as 4D-MRA for dynamic AVS evaluation is discussed in a later section.

Limitations

Despite its advantages, ASL has important constraints. The SNR is intrinsically low, and image quality is susceptible to motion artifacts and field inhomogeneities. Standard ASL provides no temporal resolution, limiting assessment to static perfusion maps rather than dynamic flow information. Although 3D fast spin-echo ASL is more resistant to susceptibility artifacts from prior hemorrhage or embolic material than susceptibility-weighted imaging (SWI), quantitative interpretation requires careful attention to post-labeling delay settings, which may need adjustment in high-flow shunting lesions, where labeled spins transit unusually rapidly.[33]

Susceptibility-weighted imaging

Principle

SWI is a high-spatial-resolution, 3D gradient-echo MRI technique that uses both magnitude and phase information to exploit magnetic susceptibility differences between tissues. The sequence is designed to maximize sensitivity to paramagnetic substances, such as deoxyhemoglobin, hemosiderin, and ferritin, which induce local magnetic field inhomogeneities and resulting signal loss. Consequently, normal venous structures typically appear hypointense because of the T2* decay caused by deoxygenated blood. Established applications of SWI in neuroradiology are extensive, ranging from the sensitive detection of cerebral microbleeds and the differentiation of calcification from hemorrhage to the evaluation of stroke, traumatic brain injury, neoplasms, and neurodegenerative disorders.[34,35]

Diagnostic performance

In the context of AVS, SWI offers distinct diagnostic advantages by providing hemodynamic information without intravenous contrast. Draining veins associated with high-flow shunts often appear hyperintense on SWI because of the TOF effect and elevated oxyhemoglobin concentration, enabling the identification of AVS and CVR/RLVD (Figure 7).[36] Conversely, SWI is highly sensitive to venous congestion, manifesting as a pseudophlebitic pattern of prominent, tortuous hypointense veins that reflects venous stasis and elevated deoxyhemoglobin.[8] A reversible hypointense focal brain sign has also been identified, indicative of parenchymal venous congestion in aggressive DAVFs. Studies report sensitivities of 73%–93% and specificities of up to 98% for detecting CVR and AV shunting compared with DSA.[26,37] Furthermore, SWI is highly valuable for post-treatment longitudinal follow-up; it can non-invasively track the prompt disappearance of cortical venous hyperintensity and the gradual resolution of hypointense venous congestion following successful DAVF

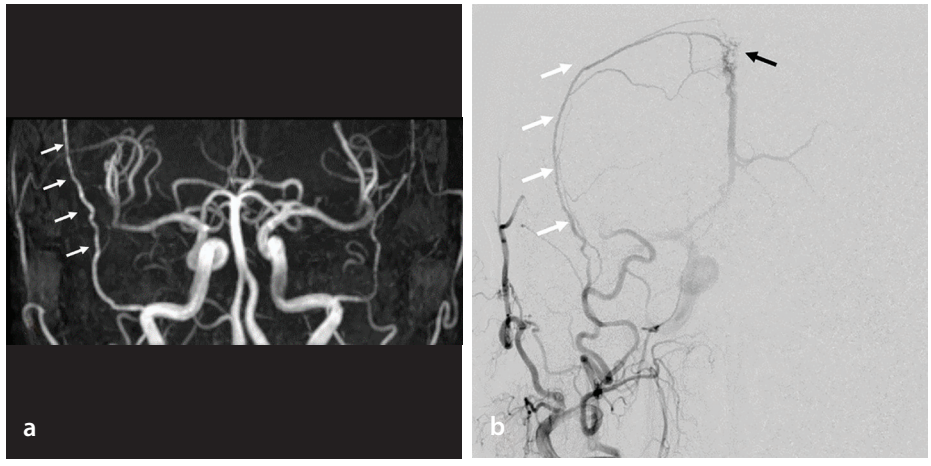

Figure 5. A 56-year-old man with a history of superior sagittal sinus thrombosis. A maximum intensity projection TOF-MRA image **(a)** demonstrates enlargement of the right middle meningeal artery branches (white arrows). Right external carotid angiography **(b)** confirms a dural arteriovenous fistula supplied by the right middle meningeal artery branches (white arrows), with early opacification of the superior sagittal sinus (black arrow). TOF-MRA, time-of-flight magnetic resonance angiography.

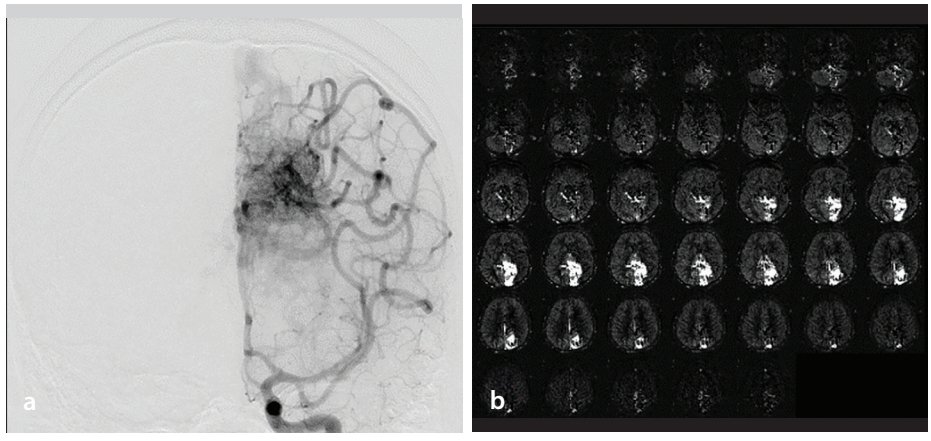

Figure 6. A 15-year-old man with a left parieto-occipital AVM (Spetzler–Martin grade IV). DSA from the left internal carotid artery injection **(a)** demonstrated the complex angioarchitecture of the AVM, fed by branches of the left anterior cerebral artery and the left middle cerebral artery. On the ASL image **(b)**, the AVM nidus was depicted as a prominent area of markedly increased signal intensity, reflecting high flow and early arterial transit. AVM, arteriovenous malformation; DSA, digital subtraction angiography; ASL, arterial spin labeling.

treatment, as well as detect RLVD recurrence.[38] For post-radiosurgery monitoring, SWI serves as a highly reliable, contrast-free alternative for tracking nidus obliteration;[39] moreover, its diagnostic accuracy can surpass that of conventional CE MRI when combined with ASL.[10]

Limitations

The primary limitation of SWI in AVS evaluation is its static nature: Like TOF-MRA, it provides no temporal resolution and cannot depict flow dynamics or distinguish arterial from venous structures based on timing alone. Susceptibility artifacts from prior hemorrhage, hemosiderin deposition, or embolic material can obscure vascular details or mimic pathologic findings.[39] Additionally, differentiation between arterialized draining veins and subacute hemorrhage may occasionally be challenging, requiring correlation with other sequences.

Recent technical innovations

In the past decade, several innovative MR techniques have been developed and are increasingly being used in clinical practice for AVS evaluation. These advances address key limitations of conventional methods, including prolonged acquisition times, suboptimal temporal resolution, high contrast agent doses, and limited hemodynamic information. This section reviews the following recent technical innovations and their clinical implications.

Ultrashort echo time magnetic resonance imaging

Various MR vendors have introduced non-contrast MRA techniques utilizing a UTE, such as Silent MRA (a non-contrast technique based on a near-zero-echo-time silent acquisition; GE Healthcare)[40] and Pointwise Encoding Time Reduction with Radial Acquisition-MRA (Siemens Healthineers).[41] The primary clinical benefit of UTE-MRA is its ability to minimize intravoxel phase dispersion, thereby preserving signal in areas of complex or turbulent flow while simultaneously reducing magnetic susceptibility artifacts caused by blood products or metallic implants. Silent MRA serves as a representative example: It combines an ASL preparation pulse with a 3D radial center-out k-space trajectory using a near-zero TE (0.016 ms), yielding angiographic images with excellent background suppression through control-label subtraction.[11]

In the clinical evaluation of cerebral AVMs, UTE-MRA has demonstrated clear superiority over conventional TOF-MRA. Silent MRA achieved a 100% detection rate compared with 79% for TOF-MRA, with a distinct benefit for micro-AVMs (nidus < 10 mm), where sensitivity remained 100% vs. 40% for TOF-MRA, translating into significantly higher Spetzler–Martin grading accuracy (79.3% vs. 38%).[41] For intracranial DAVFs, Silent MRA achieved complete agreement with DSA for fistula localization and Cognard/Borden classification, with higher sensitivity than TOF-MRA for detecting arterial feeders (87.2% vs. 79%) and draining veins (81.6% vs. 67%), and accurately predicted the accessible feeders in 96.2% of cases (Figure 8).[42]

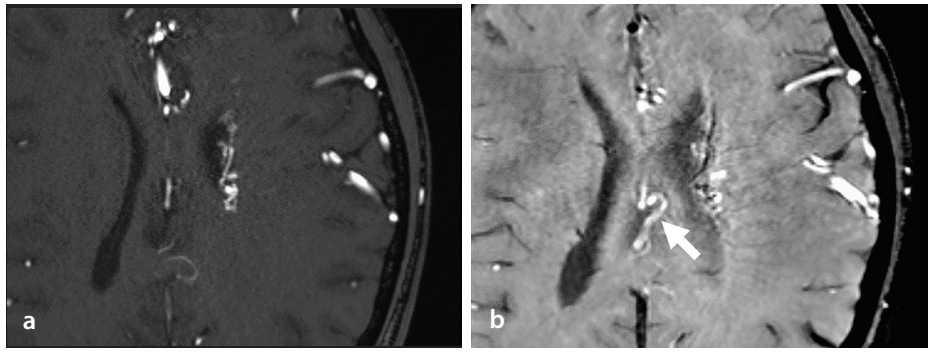

Figure 7. A 16-year-old man with a left frontal AVM (Spetzler–Martin grade IV) draining through an enlarged vein toward the internal cerebral vein. On the TOF-MRA source image **(a)**, this draining vein was not depicted, likely because of in-plane saturation related to its unfavorable orientation relative to the imaging plane. On the magnitude image of the SWI sequence **(b)**, it was clearly depicted as a prominent area of high signal intensity (arrow), allowing clear delineation of its course. TOF-MRA, time-of-flight magnetic resonance angiography; SWI, susceptibility-weighted imaging.

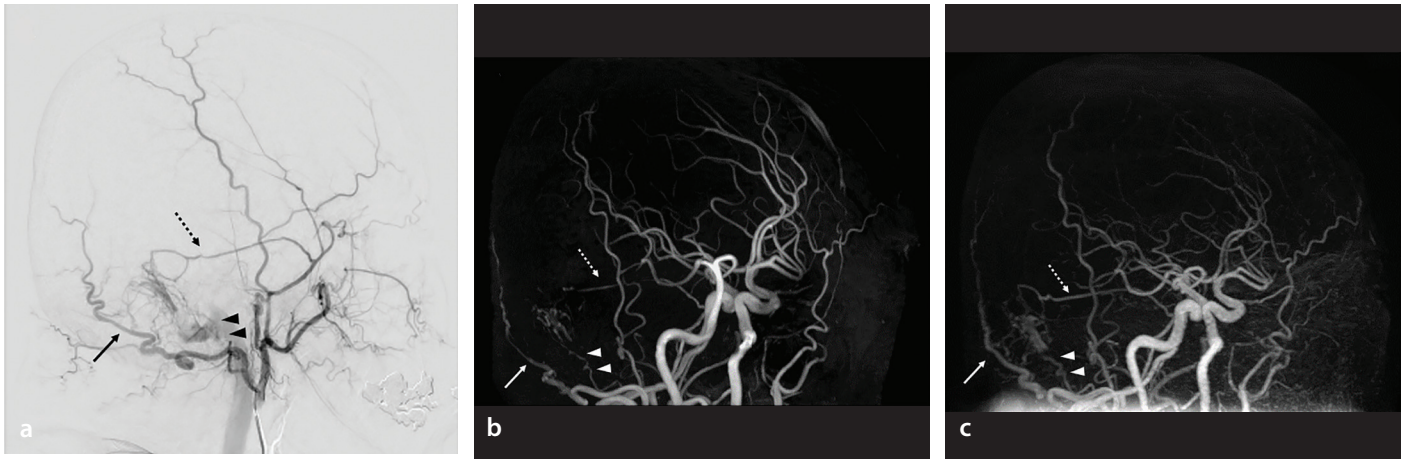

Figure 8. A 68-year-old woman with a right transverse-sigmoid sinus DAVF (Borden type **I**) supplied by three feeders: the occipital artery (arrow), the posterior auricular artery (arrowhead), and a posterior convexity branch of the middle meningeal artery (dotted arrow); the same symbols indicate the corresponding feeders in all panels. DSA from the right external carotid artery **(a)** served as the angiographic reference. On the MIP reformation of the TOF-MRA sequence **(b)**, the feeders were barely discernible. On the MIP reformation of the PETRA-MRA sequence **(c)**, the feeders were well delineated regardless of flow direction, with their distal (peripheral) portions depicted markedly better than on TOF-MRA. DAVF, dural arteriovenous fistula; DSA, digital subtraction angiography; MIP, maximum intensity projection; PETRA-MRA, Pointwise Encoding Time Reduction with Radial Acquisition-magnetic resonance angiography; TOF-MRA, time-of-flight magnetic resonance angiography.

Compressed sensing-accelerated magnetic resonance imaging (three-dimensional/four-dimensional)

Recent literature highlights the efficacy of CS techniques in 3D and 4D MRA, demonstrating reduced acquisition times, improved spatiotemporal resolution, significant dose reduction, and the capability for quantitative hemodynamic assessment.[43,44]

Compressed sensing three-dimensional magnetic resonance imaging (compressed sensing time-of-flight magnetic resonance angiography)

CS is an advanced rapid imaging technique that reconstructs high-quality images from randomly undersampled k-space data by exploiting the inherent sparsity of the images through an iterative optimization process. Because the source images of TOF-MRA predominantly consist of high-signal arteries scattered against a background of suppressed, low-signal brain parenchyma, the data are mathematically highly sparse, making them ideal for this technique. By employing sparse undersampling, CS can substantially reduce scan time compared with conventional parallel imaging, which not only minimizes the risk of motion artifacts but also makes wide-volume coverage highly feasible for routine clinical screening. Specifically, CS TOF-MRA achieves acceleration factors as high as 6.5, enabling whole-brain acquisition in approximately 2.5 minutes.[45,46] Moreover, this technique overcomes the noise limitations of conventional parallel imaging while maintaining high diagnostic accuracy for intracranial AVS. In comparative studies with DSA, CS TOF-MRA demonstrated a sensitivity of 97.3%–100% and a specificity of 94.7%–100% for AVS detection. Furthermore, it shows moderate-to-good intermodality agreement with DSA regarding the Spetzler–Martin grading of AVMs (weighted $\kappa = 0.49–0.69$), validating its utility as a rapid, non-invasive screening tool (Figure 9).[47]

Low-dose four-dimensional magnetic resonance imaging (iterative reconstruction-based time-resolved angiography with interleaved stochastic trajectories)

A critical advancement in 4D-MRA is the application of iterative reconstruction to TWIST sequences (IT-TWIST).[48] Conventional keyhole and view-sharing techniques, such as standard TWIST, improve temporal resolution by frequently acquiring the k-space center (which dictates image contrast) while dividing and sharing the undersampled peripheral k-space data across multiple adjacent time frames. However, this data sharing inevitably leads to a wider temporal footprint and greater temporal blurring. By utilizing iterative reconstruction, IT-TWIST eliminates the reliance on adjacent data sharing and can reconstruct images from a single pair of central and peripheral k-space samplings. This reduces the temporal footprint from approximately 10.3 seconds to 1.1 seconds, thereby minimizing temporal blurring and sharpening the contrast bolus profile.[49] Furthermore, the spatiotemporal regularization inherent in the iterative reconstruction process provides a profound denoising effect, significantly reducing baseline signal fluctuations. Crucially, the improved SNR resulting from both minimized blurring and robust denoising facilitates the use of substantially reduced gadolinium-based contrast agent doses. Studies indicate that IT-TWIST maintains diagnostic image quality with as little as 0.02 mmol/kg (20% of the standard dose). Although non-contrast techniques are advancing, low-dose CE approaches remain essential for patients requiring precise hemodynamic timing and high temporal resolution, where non-contrast methods may suffer from low SNR or flow-related artifacts. In clinical evaluations, low-dose IT-TWIST yielded significantly higher visualization scores for feeders, draining veins, and shunts than standard TWIST, achieving a detection sensitivity of 95.2% relative to DSA (Supplementary Videos 5 and 6).[50] This dose-reduction capability is highly favorable for patients requiring longitudinal monitoring, mitigating the risks associated with gadolinium deposition.

Golden-Angle RAdial Sparse Parallel

Golden-Angle RAdial Sparse Parallel MRI represents a synergistic integration of continuous golden-angle radial sampling and CS. Unlike conventional CE TR-MRA, which is constrained by a single contrast bolus passage, GRASP acquires k-space data continuously, allowing flexible retrospective reconstruction at any desired temporal resolution and effectively decoupling image timing from contrast kinetics. CS enables diagnostic-quality images from these highly undersampled temporal frames by exploiting spatiotemporal sparsity and applying regularization (e.g., temporal total-variation) to suppress artifacts.[24,51-53] This approach achieves isotropic 4D-MRA with temporal resolution of approximately 1–2 seconds. Furthermore, because the continuous radial sampling trajectory inherently oversamples the k-space center with each spoke, GRASP is fundamentally robust to motion and flow artifacts.[24] While gross motion is generally less problematic in neuroimaging compared with body imaging, this inherent robustness contributes to high spatiotemporal fidelity, which facilitates detailed hemodynamic assessments including vessel-specific Bolus Arrival Time mapping.[53] While specific applications to AVS are still emerging, the ability to characterize rapid flow dynamics indicates considerable promise (Supplementary Videos 7 and 8).

Arterial spin labeling-based four-dimensional magnetic resonance imaging

Although conventional ASL is established for perfusion quantification, the application of ASL as a non-contrast, TR 4D-MRA has emerged as a pivotal tool for characterizing AVMs and DAVFs. By utilizing magnetically labeled arterial blood water as an endogenous tracer, this modality offers dynamic visualization of hemodynamics comparable to DSA, but without the risks associated with radiation or exogenous contrast agents.[54]

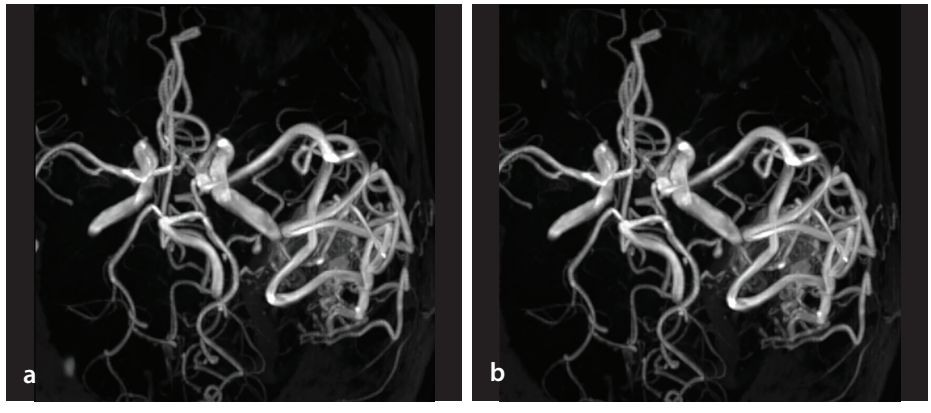

Figure 9. A 31-year-old woman with a left precentral AVM (Spetzler–Martin grade III). Both TOF-MRA **(a)** and CS TOF-MRA **(b)** visualize multiple feeders from the left middle cerebral artery, the nidus margins, and an enlarged cortical draining vein. AVM, arteriovenous malformation; TOF-MRA, time-of-flight magnetic resonance angiography; CS, compressed sensing.

Historically, PASL techniques, such as Contrast Inherent Inflow Enhanced Multiphase Angiography and standard mASTAR, initiated data acquisition immediately after a single labeling pulse (Supplementary Video 9). Although these methods achieve high temporal resolution (approximately 250 ms), they are inherently limited by the T1 relaxation of labeled spins and radiofrequency saturation, leading to signal decay in later phases. This often results in suboptimal visualization of distal draining veins, particularly in slow-flow lesions.[54]

To mitigate signal attenuation, PCASL methods, such as 4D-PACK (PCASL with CENTRA-keyhole and view-sharing), have been developed.[55] PCASL employs a longer labeling duration, maintaining a higher SNR in delayed phases and thereby improving the visualization of draining veins and collateral circulation compared with PASL.

A major limitation of standard 4D-MRA is vessel overlap. Super-selective PCASL techniques, such as 4D-S-PACK, address this limitation by labeling specific arteries (e.g., the internal carotid vs. vertebral arteries). This allows precise identification of feeding arteries and delineation of the specific vascular territories contributing to the nidus, a capability previously exclusive to DSA. In comparative studies evaluating both AVMs and DAVFs, 4D-S-PACK demonstrated superior diagnostic performance for identifying feeding arteries compared with non-selective 4D-PACK, particularly in complex multi-feeder scenarios (Figure 10).[56,57] Furthermore, recent studies have demonstrated that combining 4D-S-PACK with an interpolation algorithm (PhyZiodynamics, Ziosoft, Tokyo, Japan) and CS successfully mitigates its inherently low temporal resolution and long scan times, generating up to 61 interpolated phases and reducing scan times without sacrificing image quality.[12]

High-resolution vessel wall magnetic resonance imaging

High-resolution VW-MRI has emerged as a crucial tool for evaluating intracranial vascular pathology.[13,58] Beyond its established role in characterizing stenosis and aneurysm instability, recent evidence highlights its utility in high-flow vascular shunts by visualizing inflammatory mural remodeling that is inaccessible with conventional angiography. Black-blood techniques are essential for this assessment because they suppress high-velocity intraluminal flow signals. Advanced pulse sequences, such as Delay Alternating with Nutation for Tailored Excitation[58] and motion-sensitized driven equilibrium, minimize artifacts arising from complex shunt hemodynamics, enabling clear differentiation between true VW enhancement (VWE) and residual flow signals.

The pathophysiological basis of VWE in AVS is increasingly understood as immunothrombosis.[59] Hemodynamic stressors, such as turbulence and shunting-induced endothelial hypoxia, activate the endothelium, triggering the recruitment of innate immune cells that promote thrombosis and edema. Histopathologic data from spinal and craniovertebral DAVFs strongly support this mechanism:[60] VWE in draining veins significantly correlates with the infiltration of myeloperoxidase-positive neutrophils and lymphocytes. These enhancing veins also exhibit venous arterialization, characterized by endothelial damage and smooth muscle hyperplasia driven by high-velocity flow.[60]

Clinically, VW-MRI facilitates risk assessment and therapeutic planning. In ruptured AVMs and AVFs, VWE enables the precise identification of culprit structural irregularities, such as intranidal aneurysms or venous varices, within complex angioarchitecture, thereby guiding targeted embolization.[61,62] In unruptured lesions, VWE associated with focal edema or thrombosis may reflect an unstable inflammatory state predisposing to hemorrhage (Figure 11).[63] However, VWE can also represent persistent[64] stable vascular remodeling without an imminent risk of rupture. Therefore, although VW-MRI provides unique biological insights that complement conventional angiography, further longitudinal studies are required to determine its precise predictive value for future hemorrhagic events.

Future perspectives: artificial intelligence application

The integration of AI and deep learning (DL) has enhanced virtually every aspect of neuroimaging, from acquisition and reconstruction to quantitative analysis.[65-67] These advances are increasingly relevant to the evaluation of cerebrovascular diseases,[68,69] including AVS.

In the evaluation of AVS, the most established clinical application of DL is automated segmentation using convolutional neural networks. This approach replaces labor-intensive manual delineation with objective, reproducible morphologic metrics and has been extended to anatomically complex structures such as the AVM nidus. DL frameworks employing algorithms such as You Only Look Once[70] and U-Net (a U-shaped encoder–decoder convolutional network)[71] enable automated nidus detection and segmentation on TOF-MRA. Beyond static anatomic imaging, spatiotemporal DL models (e.g., 4DST, a 4D spatiotemporal U-Net) applied to ASL-based 4D-MRA leverage dynamic flow information to achieve superior vessel segmentation compared with spatial-only models.[72] Moreover, automated segmentation facilitates objective volumetric monitoring of radiation-induced changes following stereotactic radiosurgery, thereby aiding post-treatment management.[73]

Beyond segmentation, DL-based reconstruction (DLR) represents a complementary technology whose potential in AVS evaluation remains largely untapped. DLR can operate in the raw-data (k-space) domain,[44] the image domain,[74] or a hybrid of both.[69] These approaches reduce noise and enhance spatial resolution, enabling shorter acquisition times without loss of diagnostic quality. Applied to TOF-MRA, DLR can elevate 1.5T image quality to levels approaching those of conventional 3T imaging.[74,75] Although direct applications to AVS have yet to be reported, such improvements could broaden access to high-quality cerebrovascular assessment at lower field strengths.

Despite these promising developments, several barriers must be addressed before AI tools enter routine AVS evaluation. Most reported models have been developed and tested on small, single-institution datasets, and their generalizability across scanners, field strengths, and acquisition protocols remains insufficiently validated.[70,71] The rarity[73] and angioarchitectural heterogeneity of AVS further complicate the assembly of large, well-annotated training cohorts, and DSA-derived reference standards are themselves subject to interobserver variability.[70,71] Robust external and, ideally, prospective multicenter validation, transparent reporting, and integration into existing workflows, together with regulatory clearance, will be required before these methods can reliably support clinical decision-making.[65] For now, AI applications in AVS are best regarded as complementary research tools rather than established clinical instruments.

Non-invasive MRI evaluation of intracranial AVS has evolved considerably with recent technical innovations. Although established MRI techniques, including TOF-MRA, CE TR-MRA, SWI, and ASL, provide essential diagnostic capabilities, recent advances have

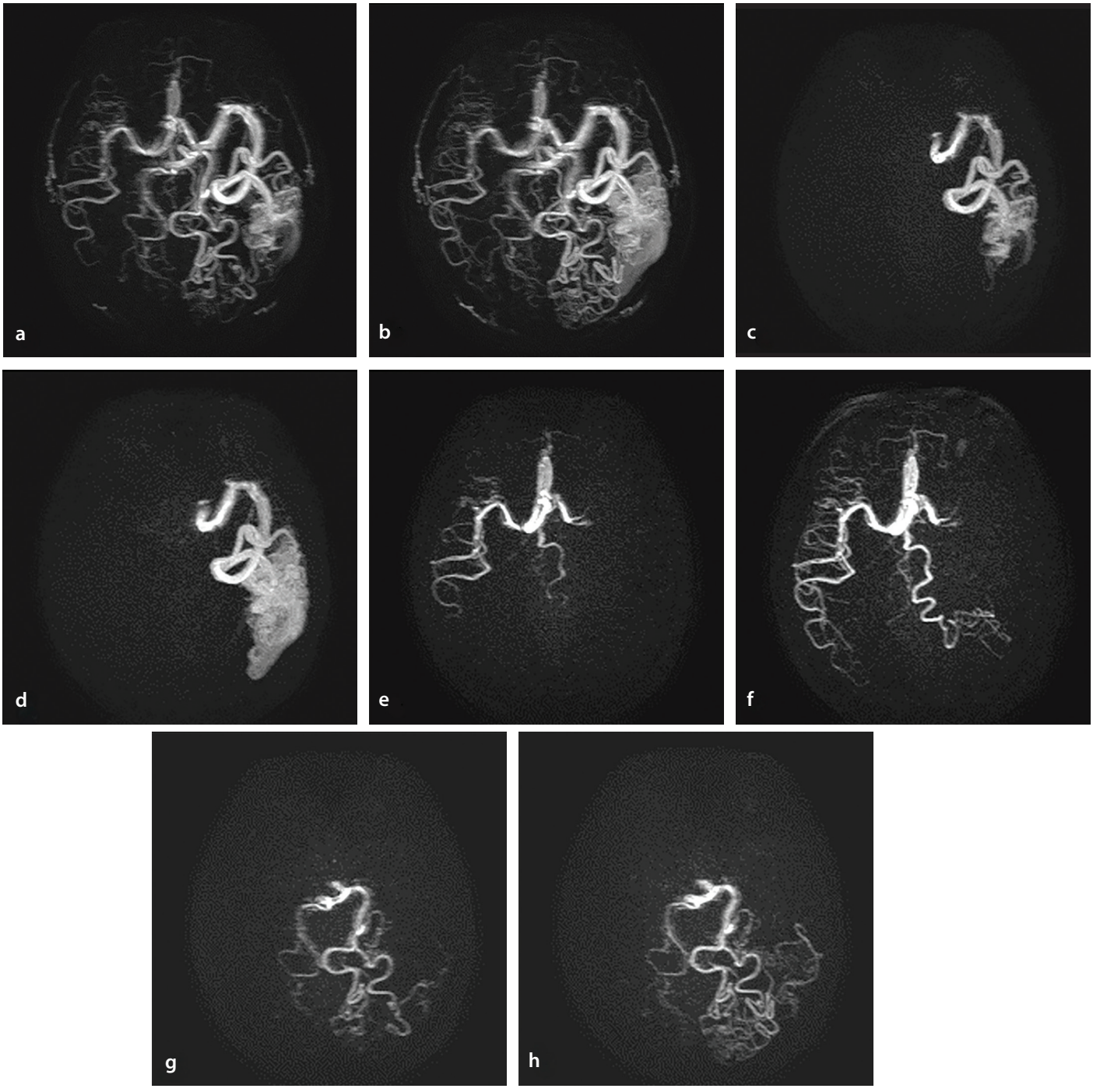

Figure 10. A man in his teens with a left parietal AVM. In ASL-based non-selective 4D-MRA (4D-PACK), gradual enhancement of the AVM nidus was demonstrated at 600 ms **(a)** and 1,200 ms **(b)**. Vessel-selective 4D-MRA (4D-S-PACK) with left MCA selection revealed the left MCA branches as the predominant feeders, with progressive enhancement of the nidus and draining vein at 500 ms **(c)** and 1,200 ms **(d)**. Additional feeders from the right ICA (**e**, 500 ms; **f**, 1,200 ms) and the vertebral artery (**g**, 500 ms; **h**, 1,200 ms) were also demonstrated (courtesy of Professor Osamu Togao, Department of Radiology, Saga University). AVM, arteriovenous malformation; ASL, arterial spin labeling; 4D-MRA, four dimensional-magnetic resonance angiography; AVM, arteriovenous malformation; MCA, middle cerebral artery; ICA, internal carotid artery.

addressed many of their intrinsic limitations. UTE MRA overcomes turbulent flow-related signal loss, CS enables high-quality acquisitions with reduced scan times and contrast doses, ASL-based 4D-MRA with vessel-selective techniques provides truly non-invasive dynamic assessment, and VW-MRI offers insights into AVS pathophysiology and potential risk stratification. Emerging AI applications demonstrate promise for automated detection and characterization.

Although DSA remains the gold standard for treatment planning and intervention, the expanding capabilities of advanced MRI techniques increasingly enable comprehensive non-invasive AVS assessment. Continued integration of these innovations promises improved patient care through earlier detection, more accurate characterization, and safer longitudinal monitoring of intracranial AVS.

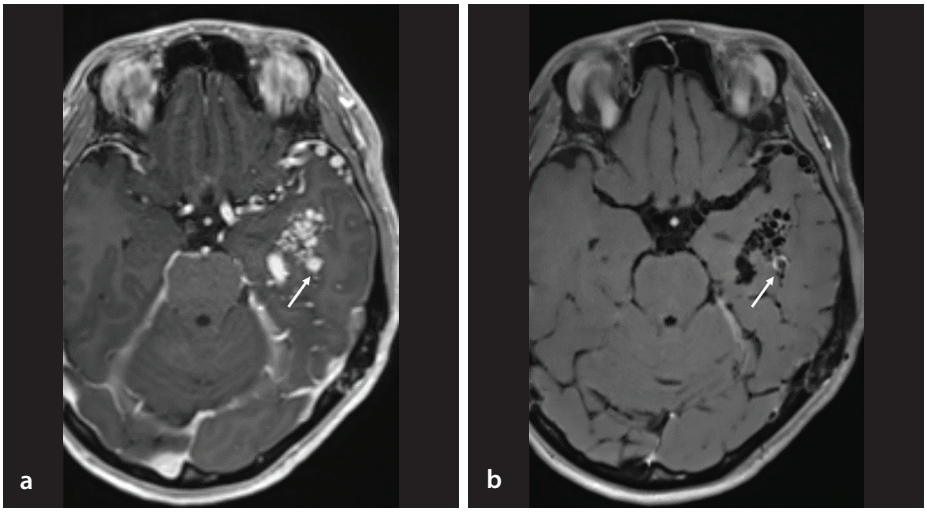

Figure 11. A 33-year-old woman with a left temporal AVM (Spetzler–Martin grade II). On the contrast-enhanced 3D T1-weighted image **(a)**, the complex angioarchitecture of the nidus, including a varix-like structure, was delineated (arrow). On the CE-DANTE-T1-SPACE sequence **(b)**, marked wall enhancement of the varix-like structure was demonstrated (arrow). AVM, arteriovenous malformation; 3D, three-dimensional.

Acknowledgement

The authors thank Professor Osamu Togao (Department of Radiology, Saga University) for kindly providing the clinical images used in this article.

Funding

This work was supported by JSPS KAKENHI Grant Number 26K10585.

Footnotes

Conflict of interest disclosure

Maya Honda receives grants from Midtown Clinic Medical Corporation. Rintaro Ito is affiliated with the Department of Innovative BioMedical Visualization, Nagoya University Graduate School of Medicine, which is financially supported by Canon Medical Systems, Inc. Mami Iima is affiliated with the Department of Fundamental Development for Advanced Low Invasive Diagnostic Imaging, Nagoya University Graduate School of Medicine, which is financially supported by HiMedic, Inc. No conflict of interest was declared by the other authors.

Supplementary Videos 1-9: https://d2v96fx-pocvxx.cloudfront.net/477dd3ac-0088-448a-a453-fd2929e03f96/content-images/ff28db6f-5b4d-42ca-acb9-62185719ac63.pdf

References

1. Alkhaibary A, Alnefaie N, Alharbi A, et al. Intracranial dural arteriovenous fistula: a comprehensive review of the history, management, and future prospective. *Acta Neurol Belg*. 2023;123(2):359-366. [Crossref]
2. Chen CJ, Ding D, Derdeyn CP, et al. Brain arteriovenous malformations: a review of natural history, pathobiology, and interventions. *Neurology*. 2020;95(20):917-927. [Crossref]
3. Spetzler RF, Martin NA. A proposed grading system for arteriovenous malformations. *J Neurosurg*. 1986;65(4):476-483. [Crossref]
4. Borden JA, Wu JK, Shucart WA. A proposed classification for spinal and cranial dural arteriovenous fistulous malformations and implications for treatment. *J Neurosurg*. 1995;82(2):166-179. [Crossref]
5. Cognard C, Gobin YP, Pierot L, et al. Cerebral dural arteriovenous fistulas: clinical and angiographic correlation with a revised classification of venous drainage. *Radiology*. 1995;194(3):671-680. [Crossref]
6. Mohr JP, Parides MK, Stapf C, et al. Medical management with or without interventional therapy for unruptured brain arteriovenous malformations (ARUBA): a multicentre, non-blinded, randomised trial. *Lancet*. 2014;383(9917):614-621. [Crossref]
7. Şentürk YE, Cantürk EM, Peker A, Yüzkan S, Peker S. Prognostic value of nidus sphericity in brain AVMs treated with Gamma Knife Radiosurgery: a preliminary study. *Diagn Interv Radiol*. 2026;32(4):510-518. [Crossref]
8. Chen Zhou ZH, Hilario A, Salvador Álvarez E, et al. The "Hypointense Focal Brain" on susceptibility-weighted imaging as a sign of venous congestion in cranial dural arteriovenous fistulas. *Neuroradiol J*. 2025;38(1):64-71. [Crossref]
9. Marchal G, Bosmans H, Van Fraeyenhoven L, et al. Intracranial vascular lesions: optimization and clinical evaluation of three-dimensional time-of-flight MR angiography. *Radiology*. 1990;175(2):443-448. [Crossref]
10. Kolahi S, Tahamtan M, Sarvari M, et al. Diagnostic performance of TOF, 4D MRA, arterial spin-labeling, and susceptibility-weighted angiography sequences in the post-radiosurgery monitoring of brain AVMs. *AJNR Am J Neuroradiol*. 2025;46(1):57-65. [Crossref]
11. Kumar S, Sharma S, Pujari VS, et al. Silent magnetic resonance angiography: techniques and applications of neurovascular imaging. *Eur J Radiol*. 2026;196:112654. [Crossref]
12. Murazaki H, Wada T, Togao O, et al. Improved temporal resolution and acceleration on 4D-MR angiography based on superselective pseudo-continuous arterial spin labeling combined with CENTRA-keyhole and view-sharing (4D-S-PACK) using an interpolation algorithm on the temporal axis and compressed sensing-sensitivity encoding (CS-SENSE). *Magn Reson Imaging*. 2024;109:1-9. [Crossref]
13. Takano K, Hida K, Tani T, Yoshimitsu K. Vasculitis syndromes: large vessel vasculitides and ANCA-associated vasculitides from a neuroradiologist's perspective. *Jpn J Radiol*. 2026;44(3):449-464. [Crossref]
14. Navot B, Hecht EM, Lim RP, Edelman RR, Koktzoglou I. MR angiography series: Fundamentals of non-contrast-enhanced MR angiography. *Radiographics*. 2021;41(5):E157-E158. [Crossref]
15. Heidenreich JO, Schilling AM, Unterharnscheidt F, et al. Assessment of 3D-TOF-MRA at 3.0 Tesla in the characterization of the angioarchitecture of cerebral arteriovenous malformations: a preliminary study. *Acta Radiol*. 2007;48(6):678-686. [Crossref]
16. Azuma M, Hirai T, Shigematsu Y, et al. Evaluation of intracranial dural arteriovenous fistulas: comparison of unenhanced 3T 3D time-of-flight MR angiography with digital subtraction angiography. *Magn Reson Med Sci*. 2015;14(4):285-293. [Crossref]
17. Buis DR, Bot JCJ, Barkhof F, et al. The predictive value of 3D time-of-flight MR angiography in assessment of brain arteriovenous malformation obliteration after radiosurgery. *AJNR Am J Neuroradiol*. 2012;33(2):232-238. [Crossref]
18. Sakamoto M, Taoka T, Iwasaki S, et al. Paradoxical parasellar high signals resembling shunt diseases on routine 3D time-of-flight MR angiography of the brain: mechanism for the signals and differential diagnosis from shunt diseases. *Magn Reson Imaging*. 2004;22(9):1289-1293. [Crossref]
19. Lee J, Lee JY, Lee YJ, et al. Differentiation of dural arteriovenous fistula from reflux venous flow on 3D TOF-MR angiography: identifying asymmetric enlargement of external carotid artery branches. *Clin Radiol*. 2020;75(9):714. [Crossref]
20. Naruto N, Kido A, Doai M, et al. Diagnosis of a dural arteriovenous fistula involving the

superior sagittal sinus: the MMA sign on routine 3D-TOF MR angiography. *Acad Radiol*. 2024;31(9):3749-3753. [Crossref]

21. Primrose CW, Hecht EM, Roditi G, et al. MR angiography series: fundamentals of contrast-enhanced MR angiography. *Radiographics*. 2021;41(4):E138-E139. [Crossref]
22. Noguchi K, Melhem ER, Kanazawa T, Kubo M, Kuwayama N, Seto H. Intracranial dural arteriovenous fistulas: evaluation with combined 3D time-of-flight MR angiography and MR digital subtraction angiography. *AJR Am J Roentgenol*. 2004;182(1):183-190. [Crossref]
23. Grossberg JA, Howard BM, Saindane AM. The use of contrast-enhanced, time-resolved magnetic resonance angiography in cerebrovascular pathology. *Neurosurg Focus*. 2019;47(6):E3. [Crossref]
24. Goldman-Yassen AE, Raz E, Borja MJ, et al. Highly time-resolved 4D MR angiography using golden-angle radial sparse parallel (GRASP) MRI. *Sci Rep*. 2022;12(1):15099. [Crossref]
25. Haller S, Zaharchuk G, Thomas DL, Lovblad KO, Barkhof F, Golay X. Arterial spin labeling perfusion of the brain: emerging clinical applications. *Radiology*. 2016;281(2):337-356. [Crossref]
26. Nabavizadeh SA, Edgar JC, Vossough A. Utility of susceptibility-weighted imaging and arterial spin perfusion imaging in pediatric brain arteriovenous shunting. *Neuroradiology*. 2014;56(10):877-884. [Crossref]
27. Lindner T, Bolar DS, Achten E, et al. Current state and guidance on arterial spin labeling perfusion MRI in clinical neuroimaging. *Magn Reson Med*. 2023;89(5):2024-2047. [Crossref]
28. Hallak H, Aljarayhi S, Abou-Al-Shaar H, et al. Diagnostic accuracy of arterial spin labeling MR imaging in detecting cerebral arteriovenous malformations: a systematic review and meta-analysis. *Neurosurg Rev*. 2024;47(1):492. [Crossref]
29. Amukotuwa SA, Marks MP, Zaharchuk G, Calamante F, Bammer R, Fischbein N. Arterial spin-labeling improves detection of intracranial dural arteriovenous fistulas with MRI. *AJNR Am J Neuroradiol*. 2018;39(4):669-677. [Crossref]
30. Hirschmann D, Marik W, Cho A, et al. Evaluation of nidus occlusion after radiosurgery in brain arteriovenous malformations-A prospective study using arterial spin labeling. *Neurosurgery*. 2026;98(1):96-104. [Crossref]
31. Thatikunta PB, Zhou LW, Lee S. Dural arteriovenous fistula presenting with decreased arterial-spin-labeling on magnetic resonance imaging. *Stroke*. 2023;54(3):e69-e70. [Crossref]
32. Mishra D, Rajamani S, Kannath SK, et al. Investigation of ASL MRI brain perfusion changes in patients with intracranial dural arteriovenous fistula following embolization and their correlation with cognitive status improvement. *J Magn Reson Imaging*. 2025;62(4):1059-1068. [Crossref]
33. Hodel J, Leclerc X, Kalsoum E, et al. Intracranial arteriovenous shunting: detection with arterial spin-labeling and susceptibility-weighted imaging combined. *AJNR Am J Neuroradiol*. 2017;38(1):71-76. [Crossref]
34. Tanaka F, Maeda M, Kishi S, et al. Updated imaging markers in cerebral amyloid angiopathy: what radiologists need to know. *Jpn J Radiol*. 2025;43(5):736-751. [Crossref]
35. Kishi S, Maeda M, Kogue R, et al. SWI brush sign of cerebral parenchymal veins in central nervous system diseases. *Jpn J Radiol*. 2025;43(5):726-735. [Crossref]
36. Miyasaka T, Taoka T, Nakagawa H, et al. Application of susceptibility weighted imaging (SWI) for evaluation of draining veins of arteriovenous malformation: utility of magnitude images. *Neuroradiology*. 2012;54(11):1221-1227. [Crossref]
37. Tritanon O, Khunvutthidee S, Kobkitsuksakul C, Jindahra P, Panyaping T. Differentiation between aggressive and benign intracranial non-cavernous dural arteriovenous fistulas using cortical venous reflux on susceptibility weighted images. *Eur J Radiol*. 2023;162(110800):110800. [Crossref]
38. Nakagawa I, Taoka T, Wada T, et al. The use of susceptibility-weighted imaging as an indicator of retrograde leptomeningeal venous drainage and venous congestion with dural arteriovenous fistula: diagnosis and follow-up after treatment. *Neurosurgery*. 2013;72(1):47-54. [Crossref]
39. Hsu CCT, Fomin I, Wray B, et al. Susceptibility weighted imaging for qualitative grading of persistent arteriovenous shunting in deep-seated arteriovenous malformations after stereotactic radiation surgery. *Neuroradiol J*. 2023;162:110800. [Crossref]
40. Miyazaki A, Nishio M, Fujita A, et al. Predicting the O'Kelly-Marotta scale score after flow-diverter stent placement using silent MRA. *Jpn J Radiol*. 2024;42(12):1403-1412. [Crossref]
41. Arai N, Akiyama T, Fujiwara K, et al. Silent MRA: arterial spin labeling magnetic resonant angiography with ultra-short time echo assessing cerebral arteriovenous malformation. *Neuroradiology*. 2020;62(4):455-461. [Crossref]
42. Prasad Balasubramanian A, Kumar Kannath S, Thomas B, Enakshy Rajan J, Kesavadas C. Comparative study of non-contrast silent and time-of-flight magnetic resonance angiographic sequences in the evaluation of intracranial dural arteriovenous fistula. *Clin Radiol*. 2024;79(3):e393-e400. [Crossref]
43. Honda M, Kataoka M, Iima M, Nickel MD, Okada T, Nakamoto Y. Ultrafast MRI and diffusion-weighted imaging: a review of morphological evaluation and image quality in breast MRI. *Jpn J Radiol*. 2025;43(11):1761-1777. [Crossref]
44. Tabo K, Kido T, Matsuda M, et al. Usefulness of compressed sensing coronary magnetic resonance angiography with deep learning reconstruction. *Jpn J Radiol*. 2025;43(11):1822-1832. [Crossref]
45. Yamamoto T, Fujimoto K, Okada T, et al. Time-of-flight magnetic resonance angiography with sparse undersampling and iterative reconstruction: comparison with conventional parallel imaging for accelerated imaging. *Invest Radiol*. 2016;51(6):372-378. [Crossref]
46. Morita K, Uetani H, Nakaura T, et al. Accelerating TOF-MRA: the impact of the combined use of compressed sensitivity encoding and spiral imaging. *Magn Reson Imaging*. 2023;103:28-36. [Crossref]
47. Sakata A, Fushimi Y, Okada T, et al. Evaluation of cerebral arteriovenous shunts: a comparison of parallel imaging time-of-flight magnetic resonance angiography (TOF-MRA) and compressed sensing TOF-MRA to digital subtraction angiography. *Neuroradiology*. 2021;63(6):879-887. [Crossref]
48. Wetzl J, Forman C, Wintersperger BJ, et al. High-resolution dynamic CE-MRA of the thorax enabled by iterative TWIST reconstruction. *Magn Reson Med*. 2017;77(2):833-840. [Crossref]
49. Yokota Y, Fushimi Y, Okada T, et al. Evaluation of image quality of pituitary dynamic contrast-enhanced MRI using time-resolved angiography with interleaved stochastic trajectories (TWIST) and iterative reconstruction TWIST (IT-TWIST). *J Magn Reson Imaging*. 2020;51(5):1497-1506. [Crossref]
50. Sakata A, Sakamoto R, Fushimi Y, et al. Low-dose contrast-enhanced time-resolved angiography with stochastic trajectories with iterative reconstruction (IT-TWIST-MRA) in brain arteriovenous shunt. *Eur Radiol*. 2022;32(8):5392-5401. [Crossref]
51. Ueno Y, Sofue K, Tamada T, et al. Comparison of golden-angle radial sparse parallel (GRASP) and conventional cartesian sampling in 3D dynamic contrast-enhanced MRI for bladder cancer: a preliminary study. *Jpn J Radiol*. 2024;42(12):1469-1478. [Crossref]
52. Shetty AS, Hoegger MJ, Das KK. Post-contrast abdominal magnetic resonance imaging of critically ill patients using compressed sensing free-breathing golden radial angle imaging. *Diagn Interv Radiol*. 2024;30(5):275-278. [Crossref]
53. Ito S, Okuchi S, Fushimi Y, et al. Bolus arrival time on dynamic contrast-enhanced magnetic resonance imaging using the Golden-angle RAdial Sparse Parallel (GRASP) technique: characteristics and clinical utility in moyamoya disease. *J Magn Reson Imaging*. 2025;62(5):1321-1333. [Crossref]
54. Gomyo M, Tsuchiya K, Yokoyama K. Noninvasive dynamic vascular imaging:

arterial spin labeling-based noncontrast magnetic resonance digital subtraction angiography for cerebral disease diagnoses. *Jpn J Radiol*. 2025;43(7):1049-1065. [Crossref]

55. Obara M, Togao O, Beck GM, et al. Non-contrast enhanced 4D intracranial MR angiography based on pseudo-continuous arterial spin labeling with the keyhole and view-sharing technique. *Magn Reson Med*. 2018;80(2):719-725. [Crossref]
56. Togao O, Obara M, Helle M, et al. Vessel-selective 4D-MR angiography using super-selective pseudo-continuous arterial spin labeling may be a useful tool for assessing brain AVM hemodynamics. *Eur Radiol*. 2020;30(12):6452-6463. [Crossref]
57. Togao O, Obara M, Kikuchi K, et al. Vessel-selective 4D-MRA using superselective pseudocontinuous arterial spin-labeling with keyhole and view-sharing for visualizing intracranial dural AVFs. *AJNR Am J Neuroradiol*. 2022;43(3):368-375. [Crossref]
58. Umehana M, Fushimi Y, Okuchi S, et al. Evaluation of meningeal lymphatic vessels with delayed contrast enhanced vessel-wall MRI in cerebral infarction. *Jpn J Radiol*. 2026;44:508-519. [Crossref]
59. Kortman H, Bhatia KD, Wälchli T, Nicholson P, Krings T. Symptomatic unruptured arteriovenous malformations: Focal edema, thrombosis, and vessel wall enhancement: a retrospective cohort study. *World Neurosurg*. 2021;152:e467-e475. [Crossref]
60. Hu X, Diao Y, Hao Z, et al. Histopathological analysis of the wall enhancement of the spinal dural arteriovenous fistulae's draining veins. *Acta Neurol Belg*. 2024;124(3):927-934. [Crossref]
61. Bhogal P, Lansley J, Wong K, et al. Vessel wall enhancement of a ruptured intranidal aneurysm in a brain arteriovenous malformation. *Interv Neuroradiol*. 2019;25(3):310-314. [Crossref]
62. Cord BJ, Renedo D, Santarosa C, et al. Vessel wall MRI in ruptured cranial dural arteriovenous fistulas. *Interv Neuroradiol*. 2021;27(4):553-557. [Crossref]
63. de Campos Filho JM, Lucifero AG, Ahumada-Vizcaíno JC, et al. Risk assessment for rupture of brain arteriovenous malformations using high-resolution black-blood magnetic resonance imaging: a single-center case series. *Neurosurg Rev*. 2024;47(1):840. [Crossref]
64. Eisenmenger LB, Junn JC, Cooke D, et al. Presence of vessel wall hyperintensity in unruptured arteriovenous malformations on vessel wall magnetic resonance imaging: pilot study of AVM vessel wall "enhancement." *Front Neurosci*. 2021;15:697432. [Crossref]
65. Fujita S, Fushimi Y, Ito R, et al. Advancing clinical MRI exams with artificial intelligence: Japan's contributions and future prospects. *Jpn J Radiol*. 2025;43(3):355-364. [Crossref]
66. Asari Y, Yasaka K, Kanzawa J, et al. Super-resolution deep learning reconstruction improves brain MRI quality and detection of metastases. *Jpn J Radiol*. 2026;44:641-649. [Crossref]
67. Ma Y, Nakajima S, Fushimi Y, et al. Deep learning reconstruction for improved image quality of ultra-high-resolution brain CT angiography: application in moyamoya disease. *Jpn J Radiol*. 2025;43(10):1634-1642. [Crossref]
68. Nishioka N, Shimizu Y, Kaneko Y, et al. Accelerating FLAIR imaging via deep learning reconstruction: potential for evaluating white matter hyperintensities. *Jpn J Radiol*. 2025;43(2):200-209. [Crossref]
69. Ikebe Y, Fujima N, Kameda H, et al. Ultra-fast whole-brain T2-weighted imaging in 7 seconds using dual-type deep learning reconstruction with single-shot acquisition: clinical feasibility and comparison with conventional methods. *Jpn J Radiol*. 2026;44(1):35-42. [Crossref]
70. Hong JS, You WC, Sun MH, et al. Deep learning detection and segmentation of brain arteriovenous malformation on magnetic resonance angiography. *J Magn Reson Imaging*. 2024;59(2):587-598. [Crossref]
71. Dong M, Xiang S, Hong T, et al. Artificial intelligence-based automatic nidus segmentation of cerebral arteriovenous malformation on time-of-flight magnetic resonance angiography. *Eur J Radiol*. 2024;178:111572. [Crossref]
72. Chung SH, Wang Z, Zhao T, et al. ASL 4D MRA intracranial vessel segmentation with deep learning U-Nets. *Magn Reson Med*. 2026;95(4):2384-2396. [Crossref]
73. Ho HH, Yang HC, Yang WX, et al. Deep learning for automated segmentation of radiation-induced changes in cerebral arteriovenous malformations following radiosurgery. *BMC Med Imaging*. 2025;25(1):218. [Crossref]
74. Omori A, Tatekawa H, Oura T, et al. Deep learning reconstruction enhances 1.5T MR angiography beyond 3T in vascular visualization for Moyamoya disease. *Jpn J Radiol*. 2026;44(6):998-1005. [Crossref]
75. Jeon YH, Park C, Lee KH, et al. Accelerated intracranial time-of-flight MR angiography with image-based deep learning image enhancement reduces scan times and improves image quality at 3-T and 1.5-T. *Neuroradiology*. 2025;67(5):1203-1213. [Crossref]